CMS Physics Analysis Summary

Contact: cms-pag-conveners-exotica@cern.ch 2022/02/23

Search for resonant and non-resonant production of pairs of identical dijet resonances in pp collisions at $\sqrt{s} = 13$ TeV

The CMS Collaboration

Abstract

A data-driven search for pairs of dijet resonances with identical mass is conducted in final states with at least four jets, and results are presented for both resonant and non-resonant production modes. The search uses 138 fb^{-1} of integrated luminosity collected by the CMS detector in proton-proton collisions at $\sqrt{s} = 13$ TeV. Distributions of the four-jet mass above 1.6 TeV, and average dijet mass above 0.35 TeV, are fit with functions to determine the backgrounds. Model independent limits, at 95 % confidence level, are reported on the production cross section of four-jet and dijet resonances. These first LHC limits on resonant pair production at high mass, are applied to a signal model of diquarks that decay into pairs of vector-like quarks, excluding diquark masses below 7.6 TeV for a particular model scenario. There are two events on the tail of the distributions, with a four-jet mass of 8 TeV and an average dijet mass of 2 TeV, resulting in a local significance of 3.9 standard deviations and a global significance of 1.6 standard deviations if interpreted as a signal. The non-resonant search excludes pair production of top squarks with masses between 0.50 and 0.52 TeV, and between 0.58 and 0.77 TeV, for supersymmetric R-parity-violating decays to quark pairs, significantly extending previous limits. Here, the most significant signal hypothesis occurs at an average dijet mass of 0.95 TeV, for which the local significance is 3.6 standard deviations and the global significance is 2.5 standard deviations.

1 Introduction

The potential to discover new physics beyond the standard model (BSM) is the motivation of searches for dijet resonances. These searches look for a pair of jets, originating from a pair of partons, coming from the decay of a new particle, X. Since the energy scale of new physics beyond the standard model is most likely large, it is natural for the new particle to be massive.

The simplest and first searches, which have been conducted many times at LHC [1–18] using strategies reviewed in Ref. [19], are for s-channel single production of dijet resonances where there is one dijet in the final state: $\mathrm{pp} \to \mathrm{X} \to jj$. Because of this simple topology, where X is produced directly from the partons in the proton and must decay to the same partons, searches for single production place tight constraints on many models of BSM physics.

The next search usually considered is s-channel pair production, where new identical mass particles are produced in pairs, either XX or $\mathrm{X}\overline{\mathrm{X}}$, and there are two dijet resonances giving four jets in the final state. For these processes there is a mediator Y, either virtual or real, of the interaction between the annihilating partons in the protons and the produced pair of X particles. This mediator is not present in the single production process, so the pair production searches explore this additional possibility for new physics. Furthermore, two modes of production of the pair of new particles are possible, resonant and non-resonant, and each mode presents a unique opportunity for discovery. We present a generic search for pairs of dijet resonances in each production mode with data corresponding to an integrated luminosity of $138\,\mathrm{fb}^{-1}$ collected in 2016–2018 with the CMS detector at the LHC, and use each search to constrain a benchmark model, as discussed below.

This search considers pairs of resolved dijet resonances, X, where both jets within each dijet resonance are individually reconstructed. This allows our resonant and non-resonant searches to be sensitive to the largest possible resonance masses: X masses greater than 0.5 TeV and Y masses greater than 2 TeV. Searches for pairs of boosted dijet resonances, which use jet substructure techniques to identify boosted resonances inside of jets, have been used to search for lower mass resonances in both resonant [20] and non-resonant [21] modes of production.

First, we consider resonant production of pairs of dijet resonances,

$$\mathrm{pp} \to \mathrm{Y} \to \mathrm{XX} \to (jj)(jj) \tag{1}$$

where the intermediate state is a massive new particle, Y, decaying to identical dijet resonances, X. As a benchmark, we consider the diquark model [22], where the intermediate state is a diquark, $\mathrm{S_{uu}}$, and the dijet resonance is a vector-like quark, χ, that decays to an up (u) quark and a gluon (g) only.

$$\mathrm{uu} \to \mathrm{S_{uu}} \to \chi\chi \to (\mathrm{ug})(\mathrm{ug}) \tag{2}$$

This scalar diquark is a good benchmark because it is produced with a large cross section, due to the high probability of finding up quarks at high fractional momentum within the proton.

This is the first time resonant production of pairs of dijet resonances at arbitrary masses has been searched for at CMS. We are further motivated to conduct this search by an event, a clear candidate for resonant production of pairs of dijet resonances, that was seen and presented by a CMS search in the dijet final state [1]. As discussed in Ref. [22], that search was not optimized for this signal and could not quantify its significance, motivating a dedicated search in the four-

jet final state. Here we present an optimized and unbiased search for resonant production of pairs of dijet resonances, exploring a wide range of four-jet and dijet masses.

Second, we consider non-resonant production of pairs of dijet resonances

$$\mathrm{pp} \to \mathrm{XX} \to (jj)(jj). \tag{3}$$

As a benchmark, we consider the R-parity violating (RPV) supersymmetric model [23], where the dijet resonance is a top squark, $\widetilde{\mathrm{t}}$, with RPV decays to down (d) and strange (s) quarks

$$\mathrm{pp} \to \widetilde{\mathrm{t}}\widetilde{\mathrm{t}}^{*} \to (\overline{\mathrm{d}}\,\overline{\mathrm{s}})(\mathrm{ds}). \tag{4}$$

Non-resonant production, and this benchmark model, have been searched for by CMS and ATLAS at $\sqrt{s} = 13\,\mathrm{TeV}$ [21, 24], $\sqrt{s} = 8\,\mathrm{TeV}$ [25, 26] and $\sqrt{s} = 7\,\mathrm{TeV}$ [27, 28].

2 The CMS detector

A detailed description of the CMS detector and its coordinate system, including definitions of the azimuthal angle ϕ and pseudorapidity η, is given in Ref. [29]. The central feature of the CMS apparatus is a superconducting solenoid of 6 m internal diameter providing an axial magnetic field of 3.8 T. Within the solenoid volume are located the silicon pixel and strip tracker, and the barrel and endcap calorimeters ($|\eta| < 3.0$), where these latter detectors consist of a lead tungstate crystal electromagnetic calorimeter and a brass and scintillator hadron calorimeter. An iron and quartz-fiber hadron calorimeter is located in the forward region ($3.0 < |\eta| < 5.0$), outside the solenoid volume. The muon detection system covers $|\eta| < 2.4$ with up to four layers of gas-ionization chambers installed outside the solenoid and embedded in the layers of the steel flux-return yoke.

3 Event reconstruction and selection

A particle-flow (PF) event algorithm aims to reconstruct and identify each individual particle in an event, with an optimized combination of information from the various elements of the CMS detector [30]. Particles are classified as muons, electrons, photons, charged hadrons, or neutral hadrons. To reconstruct jets, the anti-k_{T} algorithm [31, 32] is used with a distance parameter of 0.4, denoted as AK4 jets, as implemented in the FASTJET package [33]. At least one reconstructed vertex is required. Charged PF candidates not originating from the primary vertex are removed prior to the jet finding. The candidate vertex with the largest value of summed physics-object p_{T}^2, where p_{T} is the transverse momentum, is taken to be the primary pp interaction vertex. The physics objects are the jets, clustered using the jet finding algorithm mentioned above, with the tracks assigned to candidate vertices as inputs, and the associated missing transverse momentum, taken as the negative vector sum of the p_{T} of those jets. For jets, an event-by-event correction based on jet area [34, 35] is applied to the jet energy to remove the estimated contribution from additional collisions in the same or adjacent bunch crossings (pileup).

Events are selected using a two-tier trigger system [36]. Events satisfying loose jet requirements at the first-level (L1) trigger are examined by the high-level trigger (HLT) system. At L1 single-jet triggers that require a jet in the event to exceed a predefined p_{T} threshold are used. Triggers that require H_{T} to exceed a threshold, where H_{T} is the scalar sum of jet p_{T} for all jets in the event

with $p_T > 30\,\text{GeV}$ and $|\eta| < 3.0$, are also used. The HLT requires: $H_T > 1050\,\text{GeV}$ or at least one jet reconstructed with an increased anti-k_T distance parameter of 0.8 and $p_T > 550\,\text{GeV}$.

The jet momenta and energies are corrected using calibration factors obtained from simulation, test beam results, and pp collision data at $\sqrt{s} = 13\,\text{TeV}$. The methods described in Ref. [35] are used and all *in-situ* calibrations are obtained from the current data. Jets are required to have $p_T > 80\,\text{GeV}$ and $|\eta| < 2.5$. The four jets with the largest p_T's are defined as the four leading jets. Jet identification criteria are applied to remove spurious jets associated with calorimeter noise as well as those associated with muon and electron candidates that are either misreconstructed or isolated [37]. For all jets, we require that the component of the jet energy arising from neutral hadrons, and the component arising from photons, are each less than 90% of the total jet energy. For jets within the fiducial tracker coverage we additionally require the jet to have nonzero charged-hadron energy, and electron and muon energies to be less than 90% and 80% of the total jet energy respectively. An event is rejected if any of the four leading jets fails these jet identification criteria.

The dijet pairs are created from the four leading jets. There are three jet combinations in total: (j_1j_2, j_3j_4), (j_1j_3, j_2j_4) and (j_1j_4, j_2j_3). In the following definitions the subscripts 1 and 2 refer to the two dijet systems: dijet 1 and dijet 2. We find that the optimal pairing algorithm is the one minimizing the following measure of the $\eta - \phi$ space separations of the jets in the event:

$$\Delta R = |(\Delta R_1 - 0.8)| + |(\Delta R_2 - 0.8)| \tag{5}$$

Here ΔR_1 and ΔR_2 are the $\eta - \phi$ space separations between the jets in each dijet, defined below. This pairing algorithm was first used in the previous search for non-resonant production of pairs of dijet resonances [21]. It is motivated by the expectation that the jets from a dijet resonance will be closer together than uncorrelated jets, minimizing the separation of the jets, while the offsets of 0.8 in Eq. (5) reduces pairings where the jets overlap in $\eta - \phi$ space. After the optimal pairing of the jets is complete the events we use for the search are selected. Events are selected that satisfy:

$$\Delta R_1 = \sqrt{(\eta_{j_a} - \eta_{j_b})^2 + (\phi_{j_a} - \phi_{j_b})^2} < 2.0 \tag{6}$$

$$\Delta R_2 = \sqrt{(\eta_{j_c} - \eta_{j_d})^2 + (\phi_{j_c} - \phi_{j_d})^2} < 2.0 \tag{7}$$

where indices j_a and j_b refer to jets in the first dijet system (1), and indices j_c and j_d refer to jets in the second dijet system (2). These requirements reject background from hard multi-jet processes produced by quantum chromodynamics (QCD), which does not naturally give small separations in $\eta - \phi$ space between the jets in each dijet in a four-jet event. In addition, we require the η separation of the two dijets to satisfy:

$$\Delta\eta = |\eta_1 - \eta_2| < 1.1 \tag{8}$$

which further suppresses background from QCD t-channel production compared to the signal from s-channel production. Finally, the asymmetry in dijet mass between the two dijets is required to be small:

$$\text{asymmetry} = \frac{|m_1 - m_2|}{m_1 + m_2} < 0.1 \tag{9}$$

selecting dijet pairs of approximately equal mass, a property of pairs of identical resonances but not the QCD background. Here, m_1 and m_2 denote the reconstructed mass of each dijet pair. Throughout the paper, the small letter m denotes reconstructed dijet and four-jet masses, and the capital letter M denotes true resonance masses.

An analysis optimization procedure was performed using Monte Carlo simulations of signals and background. In addition to the optimal pairing method that minimized ΔR in Eq. (5), we also considered a second method that minimized the asymmetry, a third utilizing both ΔR and asymmetry, a fourth minimizing the difference between ΔR_1 and ΔR_2 , a fifth minimizing the sum of the average dijet mass and the difference in dijet mass, and finally a sixth method minimizing both the average dijet mass and the difference in dijet mass. We varied the thresholds for the event selection requirements in Eqs. 6–9, and found the expected signal significance at both low and high resonance masses, for both resonant and non-resonant signals. The optimal dijet pairing method and event selections, presented in Eqs. 5–9, are the ones that maximized the expected signal significance for the full analysis.

4 Analysis Strategy

Natural variables for the two searches are derived from the properties of the production processes. The two dijet resonances XX have equal mass, so one dimensional (1D) distributions of the average dijet mass $\bar{m}_{jj} = (m_1 + m_2)/2$ should be sufficient to observe the non-resonant production of this pair. Resonant pair production, $Y \to XX$, additionally produces a localized excess in a second variable, the four-jet mass m_{4j}, giving a bump in the two dimensional (2D) distribution of m_{4j} vs. $\bar{m}_{jj}$.

Shown in Fig. 1 is the 2D distribution of the observed data for m_{4j} vs. $\bar{m}_{jj}$. Near $m_{4j} \sim 8$ TeV and $\bar{m}_{jj} \sim 2$ TeV we observe two events, candidates for a resonant signal. For comparison, Fig. 1 also shows a simulation of our benchmark model of resonant pair production, for a diquark of mass 8.4 TeV and a vector-like quark mass of 2.1 TeV. The challenge in evaluating the significance of this signal, or any signal, is to understand the background. Perturbative QCD predictions of multi-jet production have too many theoretical uncertainties to reliably model this background. We instead use a data-driven approach, fitting a background parametrization to the observed data. We find this works well when it is done with a set of 1D distributions that span the 2D space.

The seemingly natural approach to binning the search, would be to construct the set of 1D distributions of the observed number of events as a function of m_{4j}, in bins of $\bar{m}_{jj}$, or vice versa. However, Fig. 1 shows that there are kinematic boundaries in the m_{4j} vs. $\bar{m}_{jj}$ plane which interfere with this approach. For example, binning in $\bar{m}_{jj}$ would produce m_{4j} distributions that are truncated and sculpted by these boundaries, which limits the range of the search variable m_{4j} and reduces the number of events available to determine the background. This binning approach is not optimal.

For the binning of both searches we define a new dimensionless variable, $\alpha = \bar{m}_{jj}/m_{4j}$, the ratio of the two defining variables of resonant production, and a measure of the boost of the two dijet systems for both production modes. Note that the data in Fig. 1 is contained within boundaries at fixed values of α. Along trajectories at fixed values of α the number of events

observed decreases smoothly with increasing m_{4j} , or increasing $\bar{m}_{jj}$. Along these trajectories of fixed α there is a wide unbiased range of m_{4j} or $\bar{m}_{jj}$ because the distributions are not sculpted or truncated by the boundaries. The ratio α is a good variable to bin the 2D data to construct a set of unbiased 1D distributions for a data-driven search.

In Figs. 2 and 3 we show the 2D distributions of the number of events, both observed in data and expected from a simulated signal, as a function of both α and the mass variable to be used for the 1D distributions of the search: m_{4j} for the resonant search, and $\bar{m}_{jj}$ for the non-resonant search respectively. The observed data for the resonant search in Fig. 2 is distributed with a uniform density in α, and for each value of α there is a wide unbiased range of m_{4j} to facilitate estimation of the background.

In addition, although the dijet pairs from a non-resonant signal are not produced at a fixed value of α, using a binning in the non-resonant search exploits the signal distribution in α. As can be seen in Fig. 3 properly reconstructed signals (i.e. pairs of dijets with average masses near the generated $\widetilde{t}$ mass) tend to be produced with high α. This is especially true for higher mass $\widetilde{t}$ pairs, and is because the lower values of α only occur if the $\widetilde{t}\widetilde{t}$ system is produced with some boost. Hence, examining the four-jet and average dijet mass distribution in bins of α is expected to significantly increase the sensitivity of both searches.

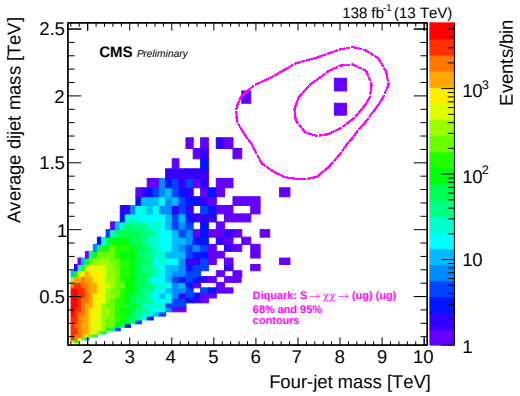

Figure 1: Number of events observed (color scale) within bins of the four-jet mass and the average mass of the two dijets. The ellipses show the 1 and 2 σ contours from a signal simulation of a diquark, with a mass of 8.4 TeV, decaying to a pair of vector-like quarks, each with a mass of 2.1 TeV.

The average dijet mass and the four-jet mass are the variables used for the signal extraction in the non-resonant and resonant search respectively, as described in more detail below. We then optimize, for maximal signal significance, both the number of α bins considered and the final observable used to search for localized excesses. The resonant search consists of thirteen simultaneous 1D searches using the m_{4j} distributions within the thirteen α bins shown in Fig. 2, and similarly the non-resonant search uses the $\bar{m}_{jj}$ distributions in the three α bins in Fig. 3. For the resonant search the lowest α value we consider is 0.1 with a bin width of 0.02 which is comparable to the reconstructed α resolution, up to an α of 0.32, and then we utilize an overflow bin for all higher α values. For the non-resonant search the optimization yielded a bin width of 0.1, for two bins between α of 0.15 and 0.35, and again a final bin is used for higher α values.

Lastly, the searches are performed above a mass threshold, for which the trigger is found to be fully efficient. In the case of the resonant analysis, the search is performed for four-jet masses $m_{4j} > 1.6$ TeV for all α values. In the case of the non-resonant analysis, the thresholds in average dijet mass vary with α: $\bar{m}_{jj}$ is required to be greater than 0.35, 0.53 and 0.61 TeV for the three

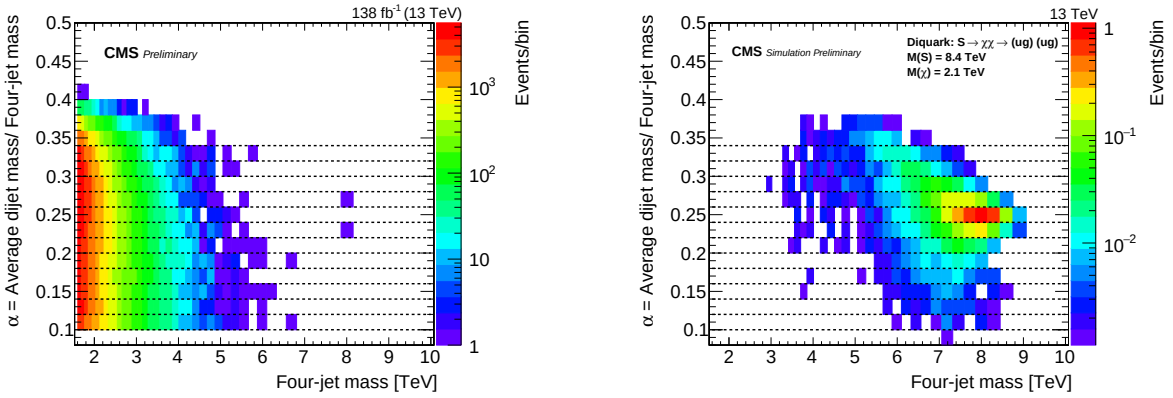

Figure 2: (Left) Number of events observed (color scale) within bins of the four-jet mass and the ratio α, which is the average mass of the two dijets divided by the four-jet mass. (Right) Number of events predicted in the same bins by a simulation of a diquark, with a mass of 8.4 TeV, decaying to a pair of vector-like quarks, each with a mas of 2.1 TeV. Both plots also show the edges of the thirteen α slices used to define the four-jet mass distributions used in the resonant search (dashed lines).

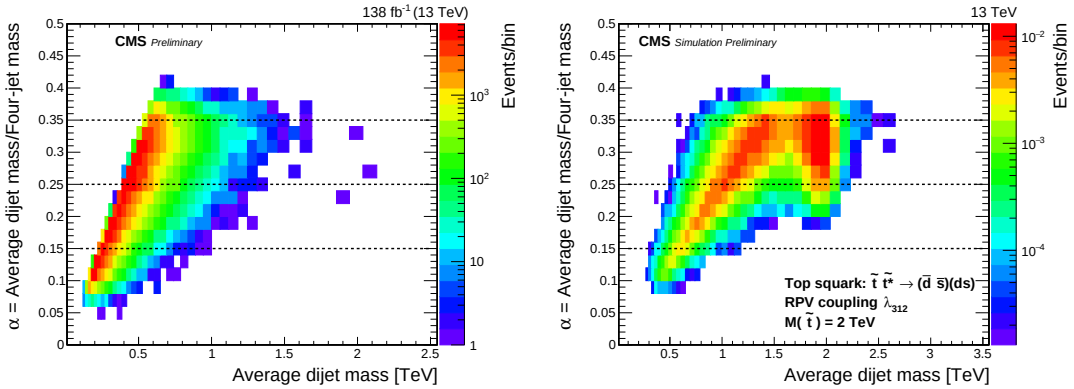

Figure 3: (Left) Number of events observed (color scale) within bins of the average mass of the two dijets and the ratio α of that mass to the four-jet mass. (Right) Number of events predicted in the same bins by a simulation of the production and R-parity violating decay of a pair of top squarks with a mass of 2 TeV. Both plots also show the edges of the three α slices used to define the average dijet mass distributions used in the non-resonant search (dashed lines).

bins with lower α edges of 0.15, 0.25 and 0.35, respectively. In Fig. 3 this requirement on $\bar{m}_{jj}$ is removed for illustrative purposes, and the same events as in Fig. 2 are shown as a function of α and $\bar{m}_{jj}$, requiring $m_{4j} > 1.6$ TeV in Fig. 3 as in Fig. 2.

5 Simulation and signal

The benchmark model for the resonant search is based on the aforementioned model of a diquark decaying to pairs of vector-like quarks, defined in Eq. (2). Specifically, we consider a scalar diquark resonance (S_{uu}) which decays to two vector-like quarks (χ), which each then decays to a quark and gluon pair: $S_{uu} \to \chi\chi \to (ug)(ug)$. The MADGRAPH 5MC@NLO [38] generator, with code specifying the model provided to us by the authors of Ref. [22], is used to generate these events and Madspin is used for the vector-like quark decay to a quark and a

gluon. We generated events for diquark masses between 2 and 9 TeV and for vector-like quark masses between 0.2 and 3.8 TeV.

The benchmark model for the non-resonant search is the pair production of top squarks defined in Eq. (3). In this RPV supersymmetry (SUSY) model [39], the top squarks decay to d and s quarks via the three-generation coupling λ''_{312} with 100% branching fraction. For this model we also use MADGRAPH 5MC@NLO to generate events and we include processes with up to one additional final state parton from initial and final state radiation. Events are generated with up to one additional jet. We produced samples with top squarks masses between 0.5 and 3 TeV. For the signal simulations, PYTHIA 8 [40] is used to produce the parton shower and the resulting final state particles, and GEANT4 [41] is used for the simulation of the particles through the CMS detector.

A background sample of QCD multijet events is also produced, for the optimization of the search and qualitative comparisons with the observed data. The generation starts from the lowest order (LO) QCD $2 \to 2$ processes of jet production, and includes additional jets from QCD initial and final state radiation within the parton shower. These background predictions are produced by the PYTHIA 8.205 program, with the CUETP8M1 tune [42, 43] using the parton distribution function (PDF) set NNPDF2.3LO [44], and also include the GEANT4-based simulation of the CMS detector.

In Fig. 4 the shapes of signals in the resonant and non-resonant searches for various S_{uu} and top squark masses respectively are shown for the α bin with the largest signal present. The distributions of four-jet mass, for signals in the resonant search, peak just below the input generator mass and have a long tail to low masses from radiation. The distributions of average dijet mass, for dijet resonances in the non-resonant search, also have a peak just below the input generator mass from correct pairings of the four jets, and an additional peak at lower masses from incorrect pairings.

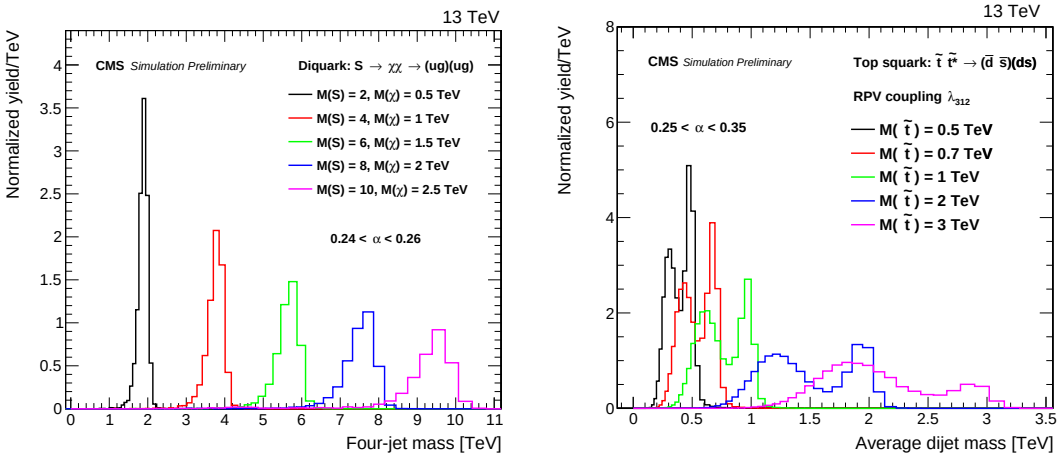

Figure 4: Signal differential distributions for the resonant search (left) as a function of four-jet mass, and the non-resonant search (right) as a function of the average mass of the two dijets, for the α slice with the largest signal yield in each search. The integral of each distribution has been normalized to unity.

The acceptance times efficiency, for signals in the resonant and non-resonant searches, are shown in Fig. 5 as a function of diquark and top squark mass. The acceptance is defined as the fraction of events passing the kinematic selection criteria. The efficiency is the fraction of events satisfying the mass selection of the search: four-jet mass cut for the resonant search,

dijet mass cut for the non-resonant search. Figure 5 also shows the signal acceptance alone, namely the relative efficiency of the kinematic selection criteria, after the mass selection is applied. The highest signal acceptance for the resonant search, with $\alpha_{\text{true}} = M(\text{X})/M(\text{Y}) = 0.25$, is naturally for the corresponding bin with $0.24 < \alpha < 0.26$. For the non-resonant search, which does not have an α_{true} or a natural value of α, the highest signal acceptance is for the bin with $0.25 < \alpha < 0.35$. The acceptance, which originates from the dijet matching and angular separation requirements of Eqs. 6–9, is approximately independent of resonance mass in both searches.

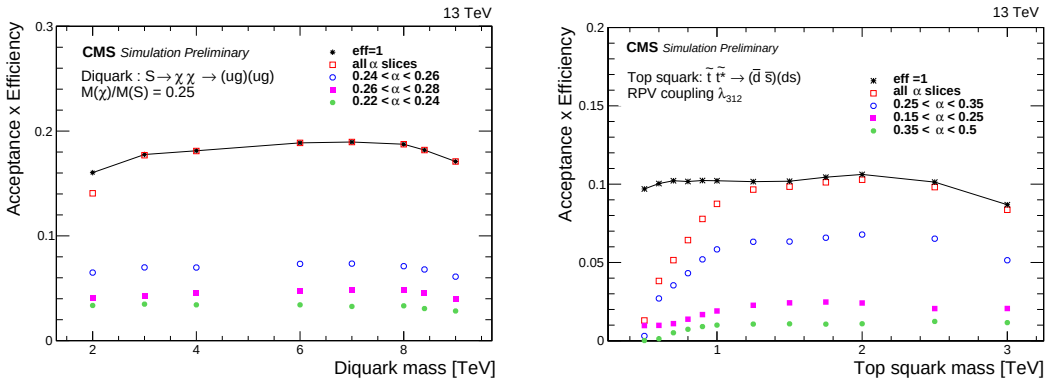

Figure 5: The acceptance times efficiency of a resonant signal vs the diquark mass (left), and a non-resonant signal vs the top squark mass (right), inclusively, i.e. for all α values, and for the three α bins that contain the majority ($\geq 85\%$) of the signal. The case when the efficiency of the mass selection is unity is also shown as a solid line.

6 Background estimation

A data-driven technique is used to estimate the background. As in previous resonance searches [3, 5–18, 45], we fit empirical functional forms to the observed mutijet mass distributions. Our primary background function, which gives the best fit to the differential cross section data without including any signal component, is the ModDijet-3p function : $\mathrm{d}\sigma/\mathrm{d}m = p_0(1 - x^{1/3})^{p_1}/x^{p_2}$, where p_0, p_1, p_2 are free parameters. Here, $x = m/\sqrt{s}$, with m being the mass used for the search, which is the four-jet mass in the resonant search and the average dijet mass in the non-resonant search. We use two alternate background functions to estimate the systematic uncertainty in the background from variations in the functional form: the Dijet-3p function, $\mathrm{d}\sigma/\mathrm{d}m = p_0(1 - x)^{p_1}/x^{p_2}$, and the PowExp-3p function, $\mathrm{d}\sigma/\mathrm{d}m = p_0 e^{-p_1 x}/x^{p_2}$.

In Fig. 6 we show the three functional forms, fitted to examples of the observed differential cross section as a function of four-jet mass, and the simulation of the QCD background, for three out of the thirteen α bins in the resonant search. All functions give a good fit to the data, and a similar prediction of the background as the LO QCD simulation, and none of these background estimates appear to account for the two events observed at a four-jet mass of 8 TeV. The three α bins also shown in Fig. 6 contain 85% of the signal for a four-jet resonance, Y, decaying to a pair of dijet resonances, X, with $\alpha_{\text{true}} = M(\text{X})/M(\text{Y}) = 0.25$, for which representative signal shapes are shown in Fig. 6. Figure 7 shows the pulls from the fit with the ModDijet-3p function for all thirteen α bins, along with the χ^2 and number of degrees of freedom of each individual fit. All the fits are good, with individual p-values ranging from 0.14 to 0.91. The combined p-value is 0.18 for a simultaneous fit of the data with the background function, including all thirteen α bins. This came from conducting a goodness-of-fit test on pseudo-experiments, utilizing a

binned saturated likelihood ratio as the test statistic. This probability, and the pulls of the individual fits, indicate that our background model gives a good description of the data overall.

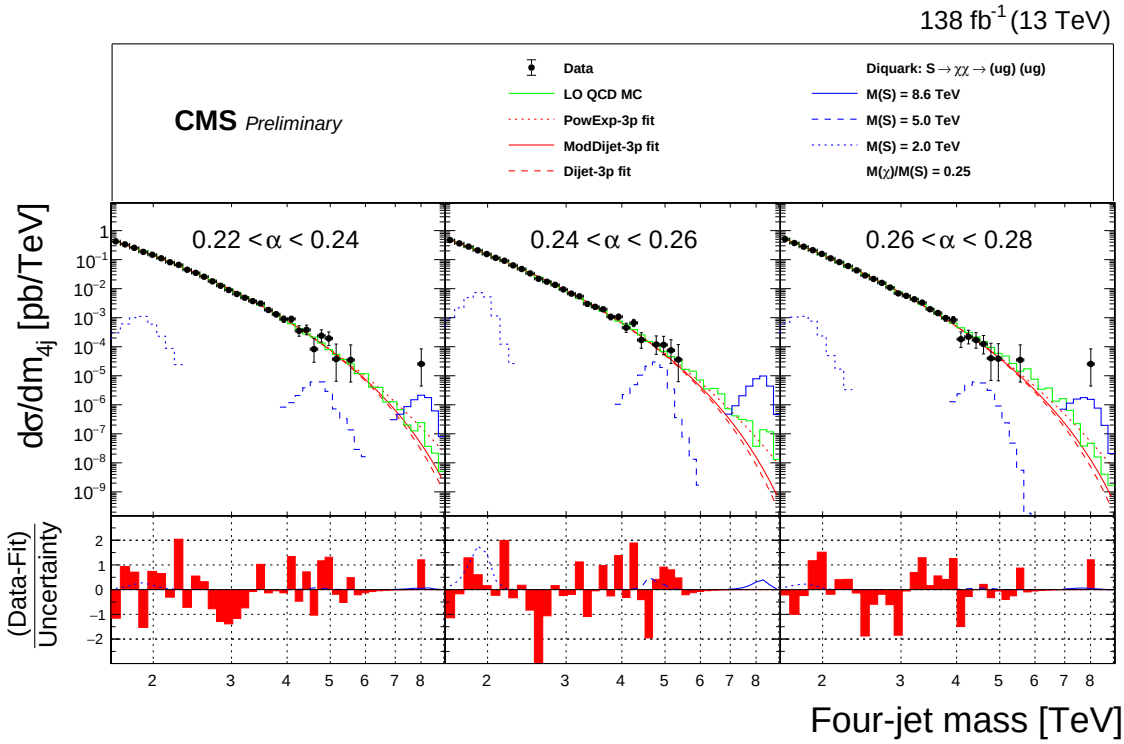

Figure 6: The four-jet mass distributions of the data (points), within three of the thirteen α bins of the resonant search, compared with LO QCD (green histogram) and fitted with three functions: a power-law times an exponential, PowExp-3p (red dotted), the standard function used by dijet resonance searches, Dijet-3p (red dashed), and a modified version of that dijet function, ModDijet-3p (red solid), each function using three parameters. Examples of predicted diquark signals are shown, with cross sections equal to the observed upper limits at 95% CL, for resonance masses of 2 (blue dotted), 5 (blue dashed), and 8.6 TeV (blue solid). The lower panel shows the pulls from the fit of the ModDijet-3p function to the data.

For the non-resonant search, Fig. 8 shows the data, fits, QCD background simulation, and signal shapes for all three α bins. The p-values of the background fits for the individual α bins range from 0.02 to 0.87, and the combined p-value, calculated with the same statistical procedure as in the resonant search, is 0.04. Here the low p-values originate from the large absolute values of the pulls, near an average dijet mass of roughly 1 TeV for $0.25 < \alpha < 0.35$ in Fig. 8. Similar pulls can also be seen in the corresponding α bins of Fig. 7, near a four-jet mass of roughly 3-4 TeV. Only the lowest α bin in the non-resonant search extends to sufficiently small values of average dijet mass to contain a noticeable peak for a 0.6 TeV top squark, as shown in Fig. 8. It is the only α bin sensitive to top squark masses between 0.5 and 0.6 TeV.

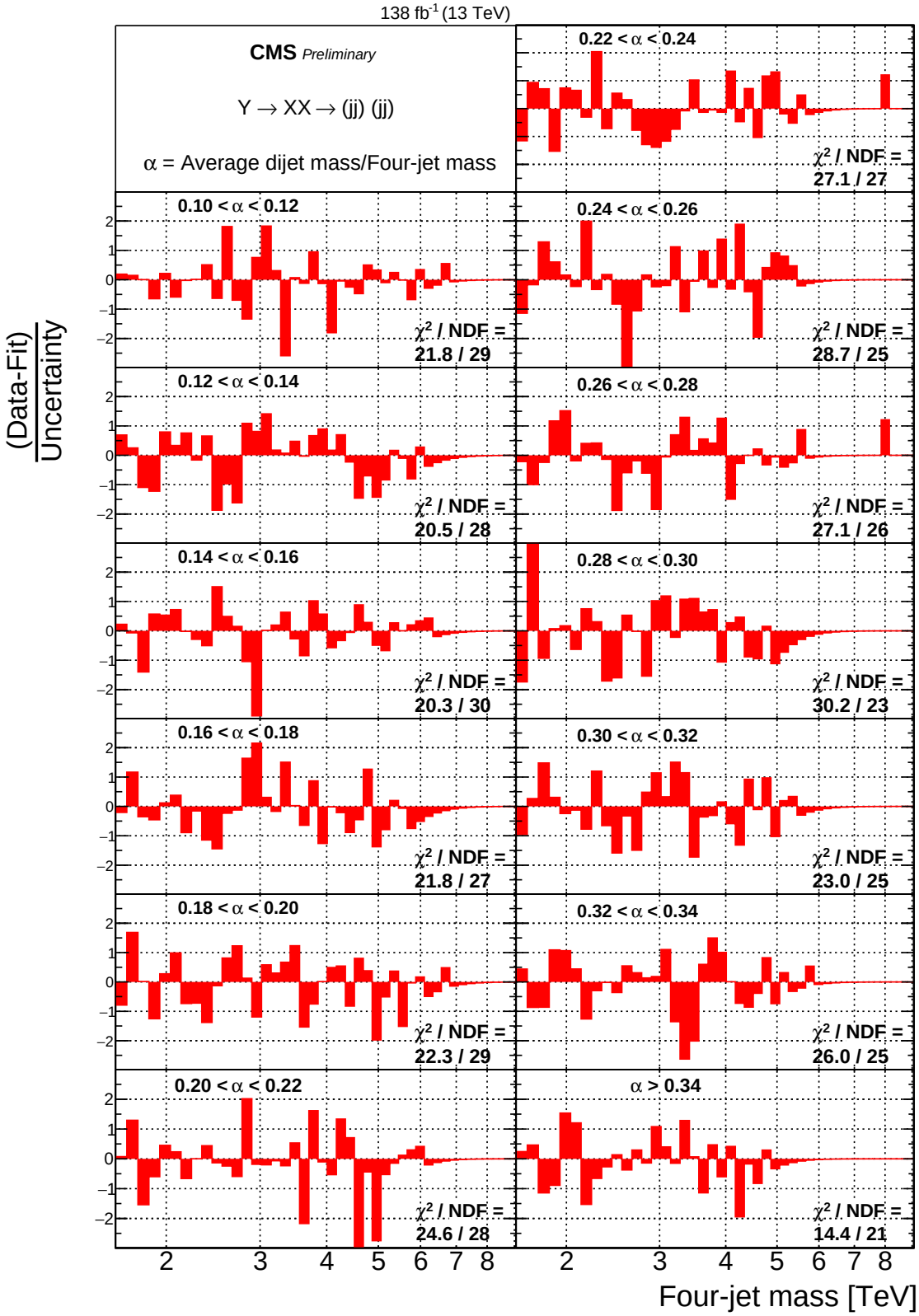

Figure 7: The pulls from the fit of the ModDijet-3p function to the four-jet mass distribution, and the goodness of fit metric χ^2/NDF, for all thirteen α bins of the resonant search. The distribution and fits are presented for three of the thirteen α bins in the previous figure. The pulls are calculated using the statistical uncertainty of the data.

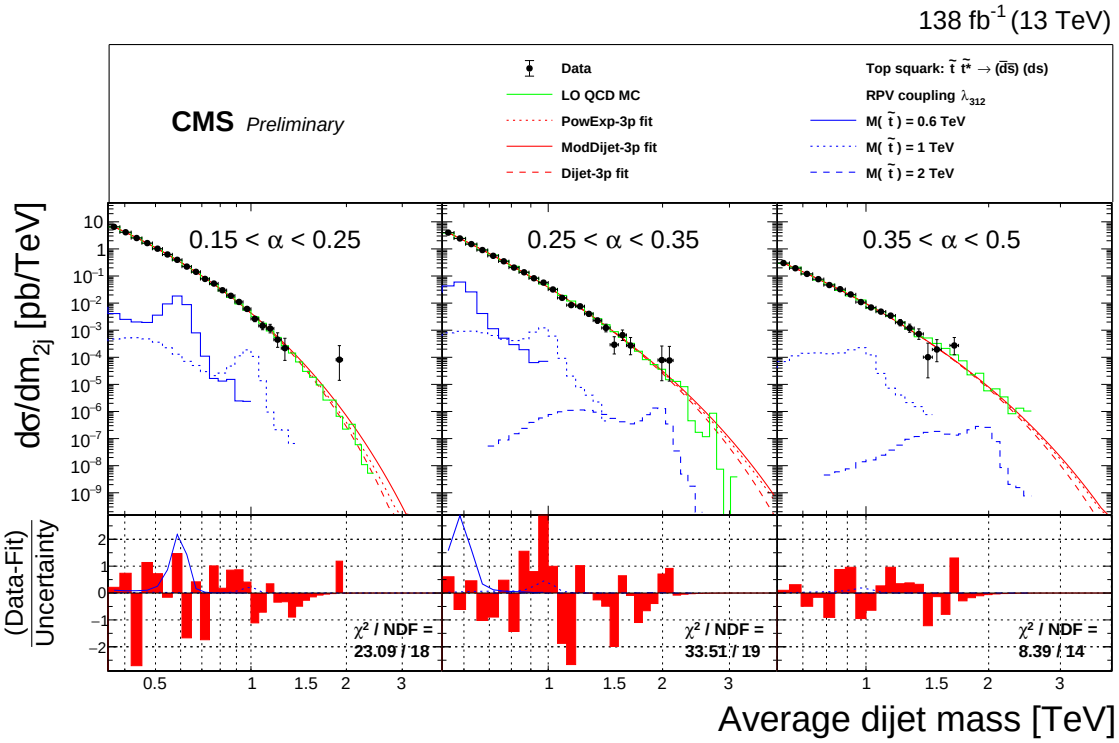

Figure 8: The average dijet mass distributions for the data (points), within the three α bins of the non-resonant search, compared with LO QCD (green histogram) and fitted with three functions: a power-law times an exponential, PowExp-3p (red dotted), the standard function used by dijet resonance searches, Dijet-3p (red dashed), and a modified version of that dijet function, ModDijet-3p (red solid), each function using three parameters. Examples of predicted top squark pair production signals are shown, with cross sections equal to the expected SUSY cross sections, for top squark masses of 0.6 (blue solid), 1 (blue dotted), and 2 TeV (blue dashed). The lower panel shows the pulls from the fit of the ModDijet-3p function to the dijet mass distribution, the aforementioned signals, and the goodness of fit metric χ^2/NDF, for all three α bins of the non-resonant search.

7 Search Results

The search is a fit of the background function plus the simulated signal shape to the data, taking into account statistical and systematic uncertainties. As discussed, the data are the four-jet mass distributions in thirteen bins of α for the resonant search, and the average dijet mass distributions in three bins of α for the non-resonant search. The fit is done simultaneously for all the bins of α within each search. The results of the search are the expected and observed upper limits on the signal cross section for all experimentally accessible values of resonance mass. For some values of resonance mass, the best fit cross section and observed statistical significance of the signal hypothesis is also of interest.

The dominant sources of systematic uncertainty on the signal modeling are the jet energy scale, the jet energy resolution, and the integrated luminosity. The main source of uncertainty in the background modeling comes from the choice of the background function, and the range of possible values of the parameters of the background function. The uncertainties with the largest impact on the extracted signal yield are the background related ones, with the signal modeling related ones being negligible. The uncertainty in the jet energy scale is within 2% for all values of the four-jet and dijet masses. This uncertainty is propagated to the limits by shifting the four-jet and dijet mass shapes for the signals by $\pm$2%. The uncertainty in the jet energy resolution translates into an uncertainty of 10% in the resolution of the four-jet and dijet masses [35], and is propagated to the limits by observing the effect of increasing by 10% the reconstructed width of the four-jet and dijet mass shapes for the signals. The total integrated luminosity has an uncertainty of 1.6%, the improvement in precision relative to Refs. [46–48] is reflecting the uncorrelated time evolution of some systematic effects, and is propagated to the normalization of the signal. Changes in the background function used, and the values of the background function parameters as estimated from the fit, can introduce changes in the signal yield. All these systematic uncertainties are included in the extracted cross section, limits and significance, as discussed in the next paragraph.

For the signal extraction, we use a multi-bin counting experiment likelihood, which is a product of Poisson distributions corresponding to different bins. We evaluate the likelihood independently at each value of resonance mass from 1.6 to 10 TeV in 100 GeV steps for the resonant search and, for the non-resonant search, in 25 GeV steps between 0.5 and 1 TeV, 50 GeV steps between 1 and 1.8 TeV, and 200 GeV steps between 1.8 and 3 TeV. These step sizes are comparable to the experimental mass resolution at the lower edge of each resonance mass interval. The sources of systematic uncertainty are implemented as nuisance parameters in the likelihood model, with Gaussian constraints for the jet energy scale and resolution, and log-normal constraints for the integrated luminosity. The parameters of the empirical functional form used to describe the background are considered as freely floating nuisances, and are automatically evaluated via profiling. The discrete profiling method [49] is used for considering the choice of the functional form as a discrete nuisance parameter, which is profiled in an analogous way to continuous nuisance parameters.

Next, we proceed in setting limits, and estimating significances. The modified frequentist criterion [50, 51] is used to set upper limits on signal cross sections, following the prescription described in Refs. [52, 53] using the asymptotic approximation of the test statistic. In cases where the small number of events would make this approximation less accurate, the limit and significance estimation with respect to the background-only hypothesis are set using the hybrid Bayesian-Frequentist approach of Ref. [54], where the test–statistic distribution is derived from pseudo-experiments.

Figures 10, 9 and 11 show the model-independent observed and expected upper limits at 95%

CL on $\sigma\,\mathcal{B}\,A$, which is the product of the cross section (σ), the branching fraction ($\mathcal{B}$), and the acceptance (A) for the kinematic requirements. Figure 10 shows the limit for resonant production, with $\alpha_{\text{true}} = 0.25$, for which the maximum significance is observed. Figure 9 shows the limits for the twelve remaining values of α_{true}, chosen as the center of each bin of α. All upper limits presented can be compared to the predictions of $\sigma\,\mathcal{B}\,A$ to determine mass limits on new particles. In Figs. 10 and 9 we compare these limits from the resonant search, to the predicted cross section times branching fraction for the scalar diquark model, multiplied by the acceptance in Fig. 5. For the prediction we use a next-to-leading order (NLO) calculation with NNPDF 3.1 parton distributions, discussed in Ref. [22], for diquark masses greater than 6 TeV. For lower diquark masses the NLO calculation is not available, so we use a MADGRAPH 5MC@NLO calculation, matched at 6 TeV to the NLO calculation by multiplying by a k−factor of 1.47. In Fig. 11 the top squark signal cross section, from a simplified topology, is calculated by the LHC SUSY cross section working group at NLO including next-to-leading logarithms [55, 56].

For a given model, new particles are excluded at 95% CL in mass regions where the theoretical prediction lies at or above the observed upper limit for the appropriate final state of Figs. 9 - 11. From Fig. 9, the 95% CL lower bound on the mass of a benchmark model of a diquark, for α_{true} values between 0.11 and 0.42, varies between 7.9 and 6.7 TeV (observed), and between 7.9 and 6.4 TeV (expected), respectively. From Fig. 10, for $\alpha_{\text{true}} = 0.25$ we exclude at 95% CL diquark masses less than 7.6 TeV (observed) and 7.8 TeV (expected). These limits are for a benchmark choice of coupling values of the diquark to pairs of up quarks, $y_{\text{uu}} = 0.4$, and to pairs of vector-like quarks, $y_{\chi} = 0.6$, and other choices of the coupling values can yield different values for the diquark cross sections and the mass limits. From Fig. 11, we exclude at 95% CL top squarks with masses between 0.50 and 0.52 TeV, and between 0.58 and 0.77 TeV (observed), and less than 0.67 TeV (expected).

The observed limits in the resonant and the non-resonant search are highly correlated, because they use the same events to search for localized excesses (bumps), though they search for different signals. Figure 11 shows that in the non-resonant search, at a dijet resonance mass of roughly 0.95 TeV, the observed limit is more than 2 standard deviations above the expected limit. This is the direct result of the pulls near an average dijet mass of 1 TeV for $0.25 < \alpha < 0.35$ in Fig. 8 which resulted in a low p-value for the background fit, as previously discussed. There is a correlated effect in the resonant search. In Fig. 9 we see that the observed limit is also more than 2 standard deviations above the expected limit for a four-jet resonance mass between 3 and 4 TeV for $\alpha_{\text{true}} = 0.27$, 0.29 and 0.31.

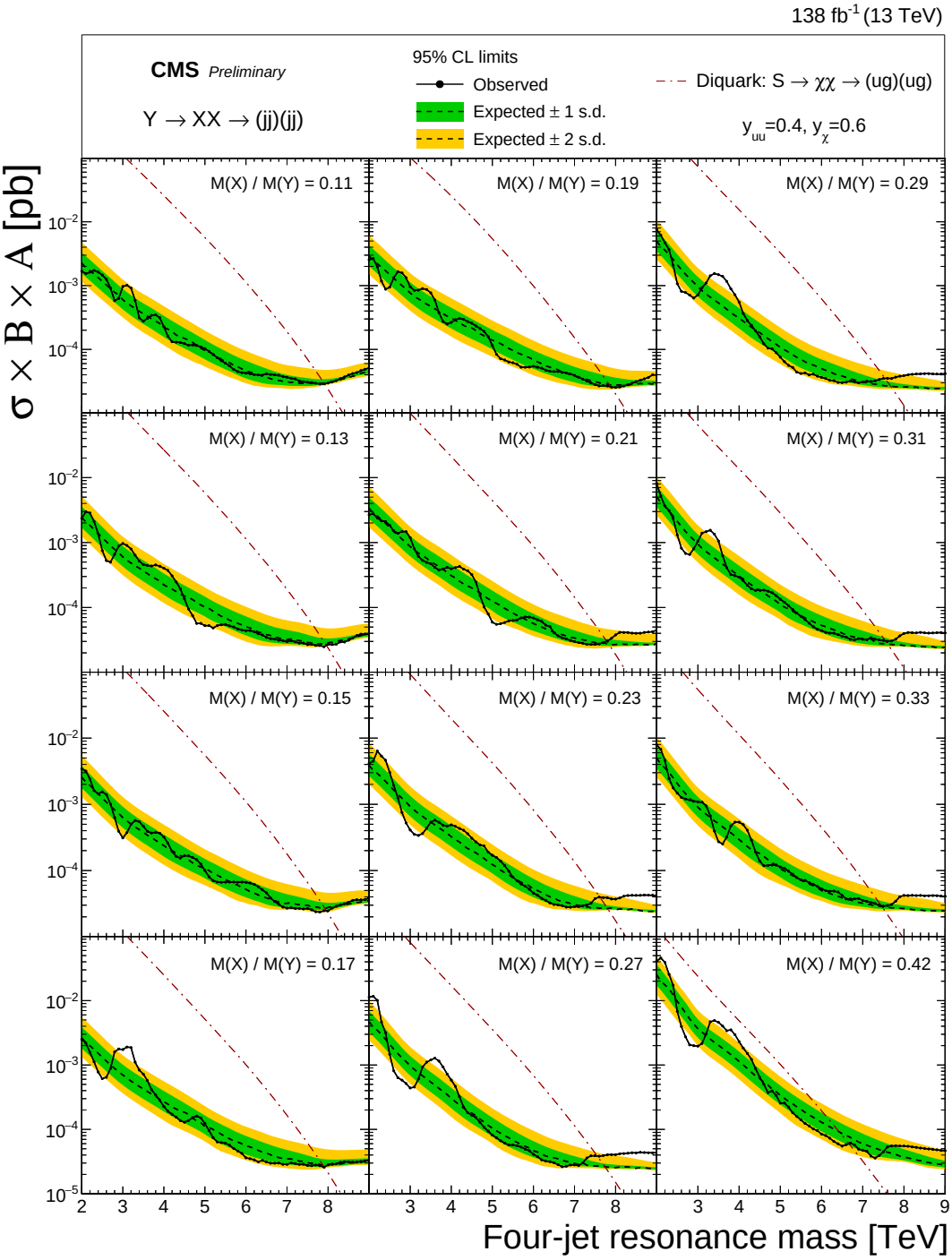

Figure 9: The observed 95% CL upper limits (points) on the product of the cross section, branching fraction, and acceptance for resonant production of paired dijet resonances decaying to a quark-gluon pair, with the values of $\alpha_{\text{true}} = M(\text{X})/M(\text{Y})$ shown. The corresponding expected limits (dashed) and their variations at the 1 and 2 standard deviation levels (shaded bands) are also shown. Limits are compared to the scalar diquark model (arXiv:1810.09429) cross section (dot dashed).

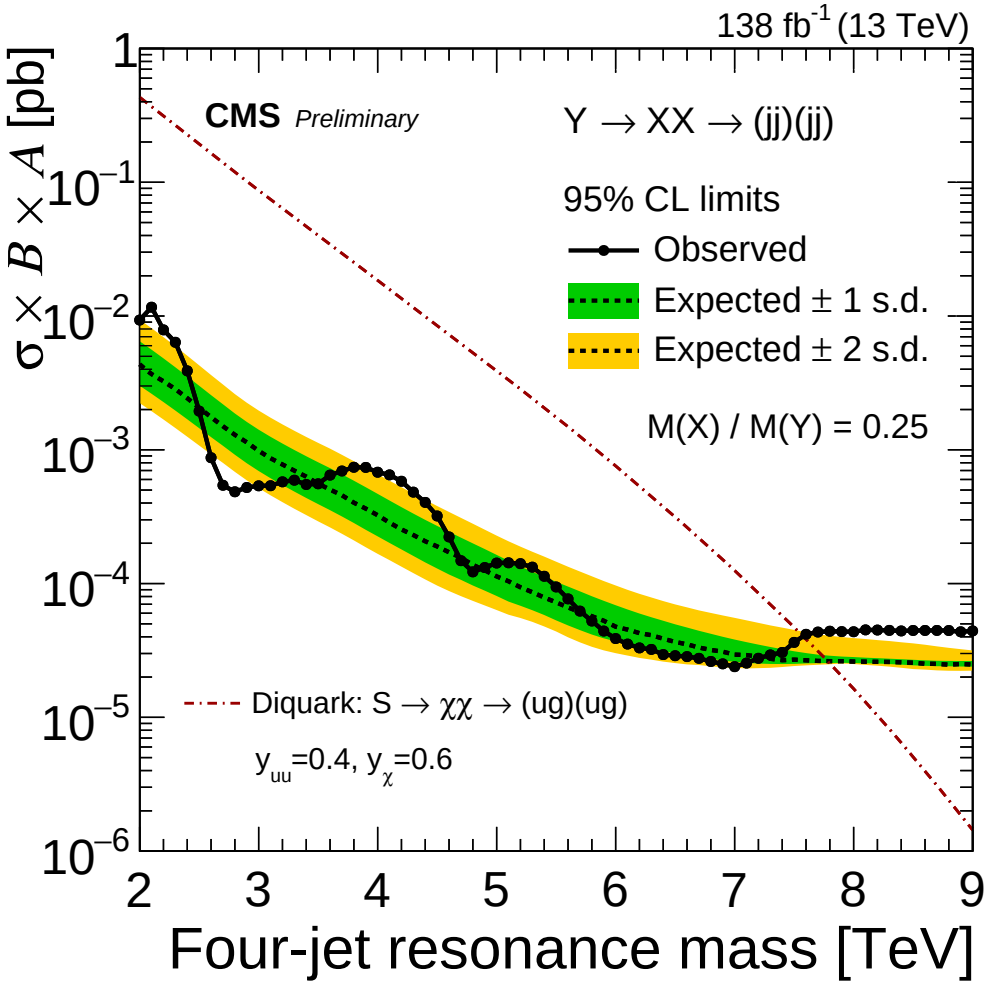

Figure 10: The observed 95% CL upper limits (points) on the product of the cross section, branching fraction, and acceptance for resonant production of paired dijet resonances decaying to a quark-gluon pair, with $\alpha_{\text{true}} = M(\text{X})/M(\text{Y}) = 0.25$. The corresponding expected limits (dashed) and their variations at the 1 and 2 standard deviation levels (shaded bands) are also shown. Limits are compared to the scalar diquark model (arXiv:1810.09429) cross section (dot dashed).

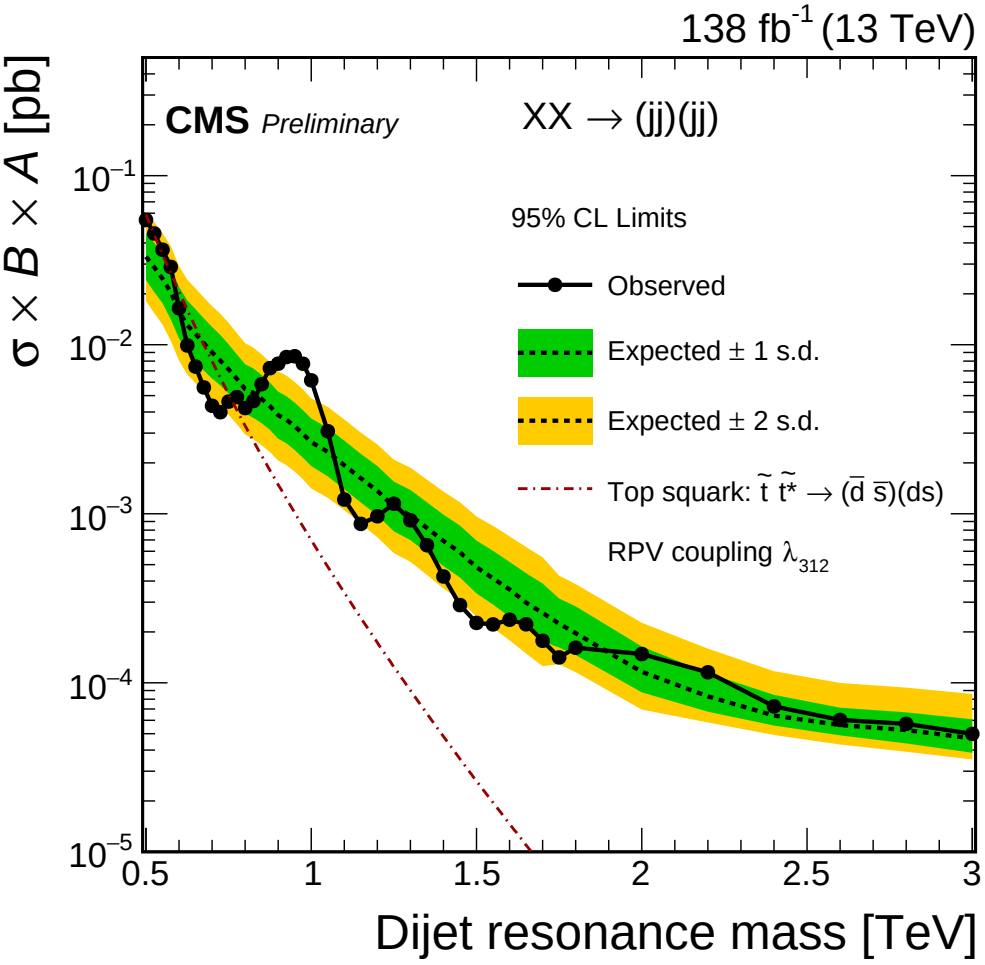

Figure 11: The observed 95% CL upper limits (points) on the product of the cross section, branching fraction, and acceptance for the non-resonant production of top squark pairs in the RPV SUSY decay scenario. The corresponding expected limits (dashed) and their variations at the 1 and 2 standard deviation levels (shaded bands) are also shown. Limits are compared to the top squark model cross section (dot dashed).

For the non-resonant search, Fig. 12 shows the local p-value as a function of dijet resonance mass. The most significant signal hypothesis occurs at a dijet resonance mass of 0.95 TeV, for which the local significance is 3.6 standard deviations and the global significance is 2.5 standard deviations. Here the global significance takes into account the look-elsewhere effect (LEE), using pseudo-experiments to calculate the probability of the background hypothesis to produce a signal-like effect with at least the observed local significance, anywhere within the sensitive range of dijet resonance mass.

For the resonant search, Fig. 13 shows the local p-value as a function of four-jet resonance mass with $\alpha_{\text{true}} = 0.25$. The most significant signal hypothesis occurs at a four-jet resonance mass of 8.6 TeV and a dijet resonance mass of 2.1 TeV, for which the local significance is 3.9 standard deviations and the global significance is 1.6 standard deviations. Here again the global significance takes into account the LEE, using pseudo-experiments as described for the non-resonant search, but the LEE for the resonant search considers a significantly larger number of possible signals, because of the two-dimensional sensitive range of four-jet resonance mass and α_{true}. At a four-jet resonance mass of 8.6 TeV the best fit value of $\sigma\,\mathcal{B}\,A$ is $(1.56^{+1.40}_{-0.87})\cdot 10^{-5}$ pb, which corresponds to $2.1^{+2.0}_{-1.2}$ events. The second largest local significance is 2.9 standard deviations, for a four-jet resonance mass of ~ 3 TeV and $\alpha_{\text{true}} = 0.17$. We note that the LEE assumes equal significance to an effect for any value of resonance mass, and the resonance width being smaller in absolute units at low masses yields higher probability for an effect within the low mass region.

This high local significance, and corresponding global significance, is predominantly caused by the two events which we previously identified, and we discuss them in more detail here and in the next two paragraphs. They are in Fig. 1, with a four-jet mass of roughly 8 TeV and an average dijet mass of roughly 2 TeV, and in Fig. 2 with the same four-jet mass. To better visualize the comparison of this small number of events to the distributions of the rest of the events, the background, and the signal hypothesis, we show in Fig. 14 the inclusive four-jet mass distribution corresponding to the sum of all thirteen α bins. This sums the two events which appear in Fig. 6 in two separate plots corresponding to α bins with $0.22 < \alpha < 0.24$ and $0.26 < \alpha < 0.28$. In this case, the background-only fits are performed using the same functional forms, but with five parameters due to the larger statistics. Hence, a ModDijet-5p : $\mathrm{d}\sigma/\mathrm{d}m = p_0(1-x^{1/3})^{p_1}/(x^{p_2+p_3\log x+p_4\log^2 x})$, a Dijet-5p : $\mathrm{d}\sigma/\mathrm{d}m = p_0(1-x)^{p_1}/(x^{p_2+p_3\log x+p_4\log^2 x})$, and a PowExp-5p function : $\mathrm{d}\sigma/\mathrm{d}m = p_0 e^{-p_1 x-p_2 x^2-p_3 x^3}/x^{p_4}$ are being utilized, where $x = m/\sqrt{s}$, with m being the four-jet mass.

The first event, shown in Fig. 15, was collected during 2017, and has a four-jet mass of 8.0 TeV, while the invariant mass of both dijet pairs is 1.9 TeV. The p_{T} of the first dijet pair, composed of jets labeled 1 and 3, is 3.5 TeV, and the second pair, consisting of jets 2 and 4, also has a p_{T} of 3.5 TeV. The two dijet pairs are back-to-back in azimuthal angle ($|\Delta\phi| = 3.1$), nearby in pseudorapidity ($|\Delta\eta| = 0.4$) and have a small mass asymmetry of 0.005. The two AK4 jets in each pair have a small distance with each other in the $\eta - \phi$ plane ($\Delta R_1 = 1.0, \Delta R_2 = 1.0$), and the p_{T}, η and ϕ of each AK4 jet are shown in Fig. 15. This event was identified by a previous dijet resonance search [1], and provided some of the motivation for this search. Since the previous search, a re-calibration of the jet energy scale caused the transverse momenta and mass values presented for this event to increase by roughly 1%.

The second event, shown in Fig. 16, was collected during 2018, and has a four-jet mass of 7.9 TeV, while the invariant mass of the first dijet pair that includes jets 1 and 4 is 2.0 TeV, and the mass of the second pair from jets 2 and 3 is 2.1 TeV. The two dijet pairs are back-to-back in azimuthal angle ($|\Delta\phi| = 3.1$), nearby in pseudorapidity ($|\Delta\eta| = 1.06$), and have a mass asymmetry of 0.02. The ΔR_1 and ΔR_2 values between the two AK4 jets in the two dijet pairs

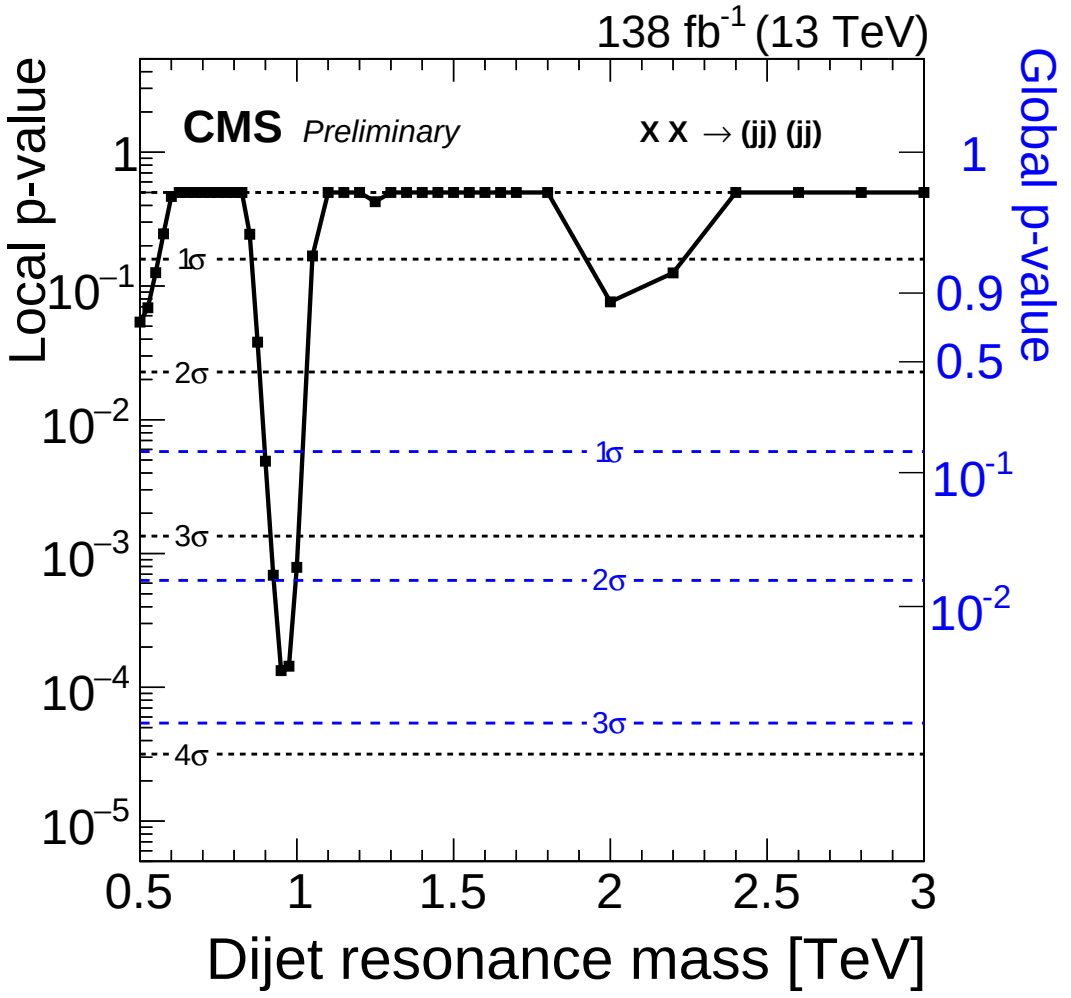

Figure 12: Observed p-values (points) for non-resonant production of a paired dijet resonance, X. The vertical scales indicate the local p-value (left axis) and the global p-value (right axis in blue) for a signal over all alpha bins. Also shown are corresponding levels of local significance (dashed) and global significance (blue dashed) in units of standard deviation (σ).

are 1.5 and 1.3. Again, the p_{T}, η and ϕ of each AK4 jet can be seen in Fig. 16.

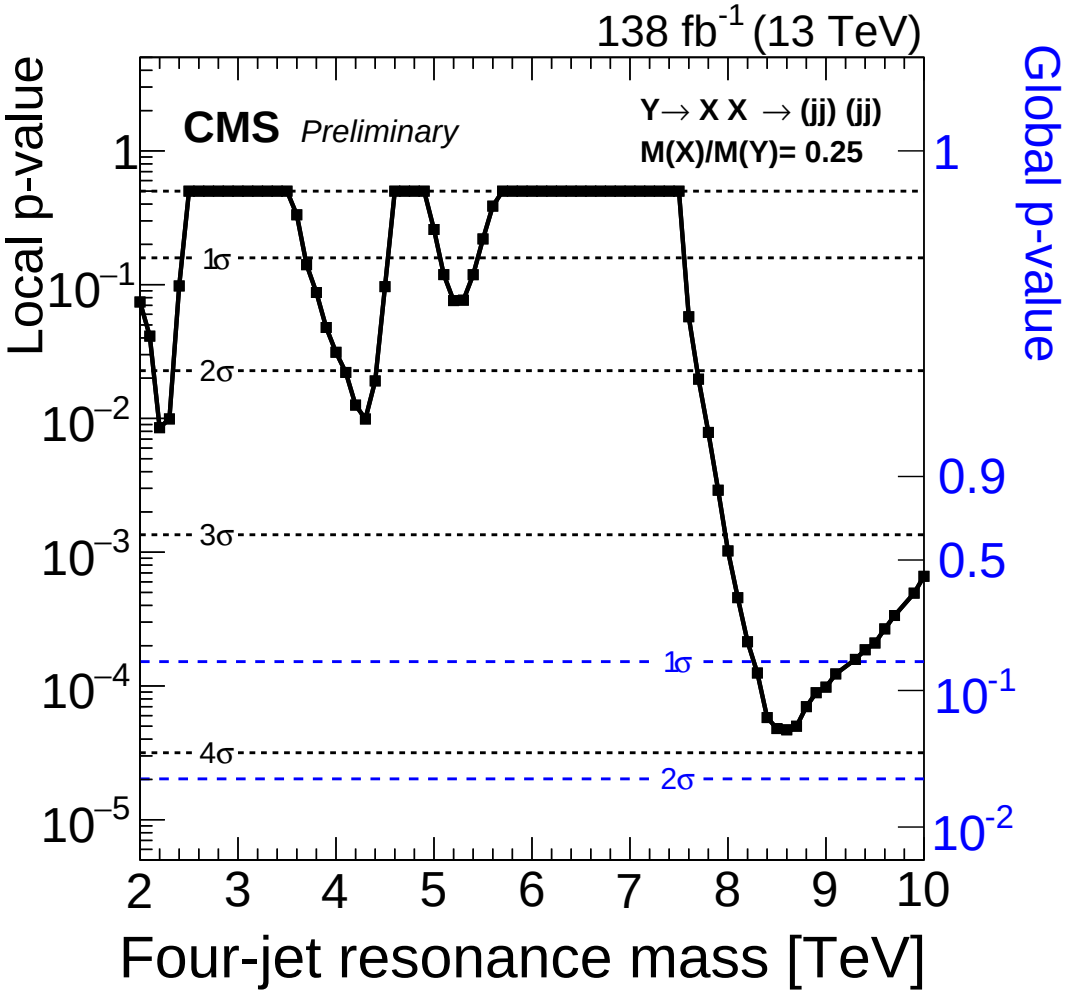

Figure 13: Observed p-values (points) for a four-jet resonance, Y, decaying to a pair of dijet resonances, X, with $\alpha_{true} = M(X)/M(Y) = 0.25$. The vertical scales indicate the local p-value (left axis) and the global p-value (right axis in blue) for a signal over all alpha bins. Also shown are corresponding levels of local significance (dashed) and global significance (blue dashed) in units of standard deviation (σ).

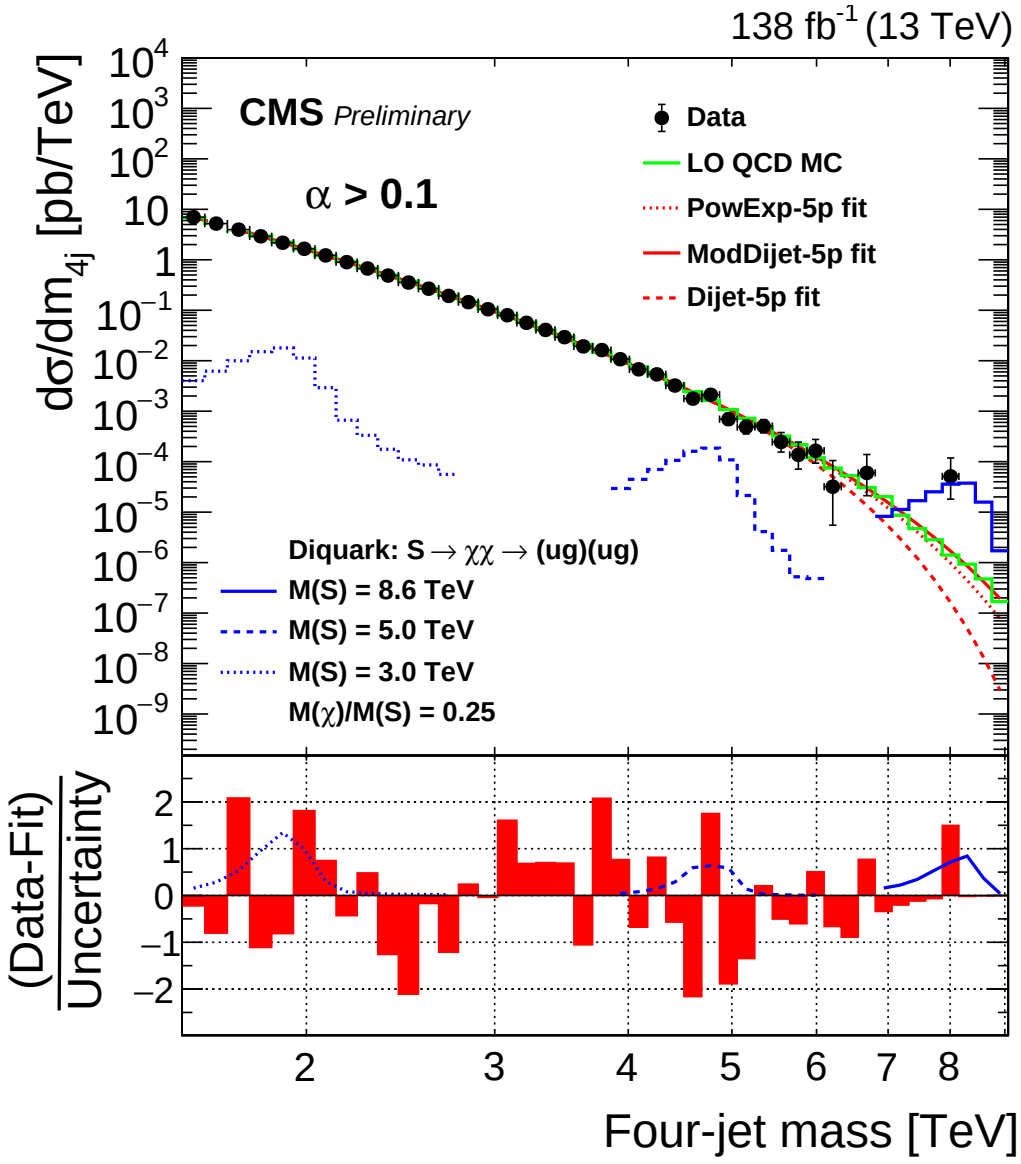

Figure 14: The four-jet mass distributions of the data (points) for all α bins together. The data is compared with a lowest order QCD prediction of jet production from PYTHIA 8 (green histogram) and fitted with three functions: a power-law times an exponential, PowExp-5p (red dotted), the standard function used by dijet resonance searches, Dijet-5p (red dashed), and a modified version of that dijet function, ModDijet-5p (red solid), each function using five parameters. Examples of predicted diquark signals, with cross sections equal to the observed upper limits at 95% CL, are shown for resonance masses of 2 (blue dotted), 5 (blue dashed), and 8.6 TeV (blue solid). The lower panel shows the pulls from the fit of the modified dijet function to the data.

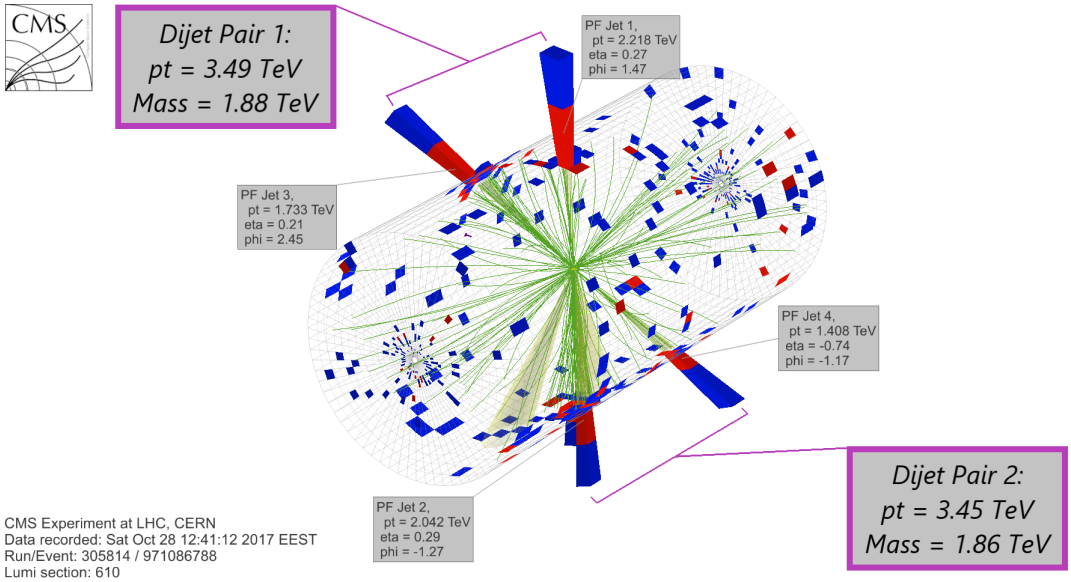

Figure 15: Three–dimensional display of the event with the highest four-jet mass of 8.0 TeV. The display shows the energy deposited in the electromagnetic (red) and hadronic (blue) calorimeters and the reconstructed tracks of charged particles (green). The grouping of the four observed jets into two dijet pairs (purple) is discussed in the text.

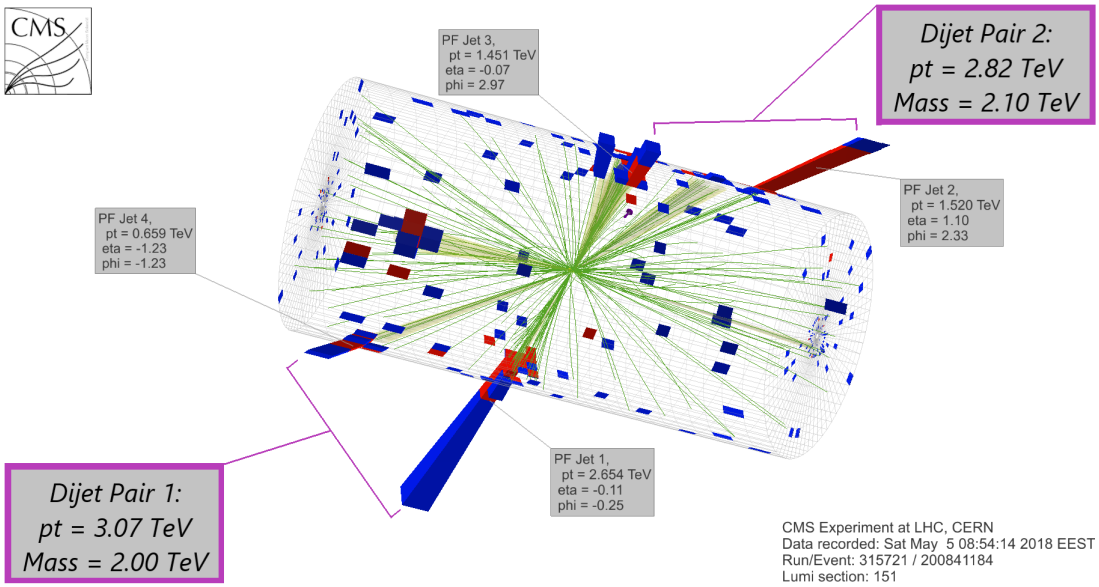

Figure 16: Three–dimensional display of the event with the second highest four-jet mass of 7.9 TeV. The display shows the energy deposited in the electromagnetic (red) and hadronic (blue) calorimeters and the reconstructed tracks of charged particles (green). The grouping of the four observed jets into two dijet pairs (purple) is discussed in the text.

8 Summary

A search for paired dijet resonances is presented in final states with at least four jets, probing dijet masses above 0.35 TeV and four-jet masses above 1.6 TeV. The search uses data from proton-proton collisions at $\sqrt{s} = 13$ TeV, collected by the CMS experiment at the LHC, corresponding to an integrated luminosity of 138 fb^{-1}.

For the first time, we search for resonant production of pairs of dijet resonances, where a massive intermediate state leads to an additional four-jet resonance in the final state. We also continue the search for non-resonant production of pairs of equal mass dijet resonances at the LHC. Empirical functions that model the background, and simulated shapes of resonance signals, are fit to the observed four-jet and dijet mass distributions. There are two events on the tail of the distributions, with a four-jet mass of 8 TeV and an average dijet mass of 2 TeV. They result in a local significance of 3.9 standard deviations and a global significance of 1.6 standard deviations, when interpreted as a signal of a four-jet resonance with mass 8.6 TeV and a dijet resonance with mass 2.15 TeV. More data are needed to establish these two events as the first hints of a signal, and LHC data with the highest possible collision energy would be the most effective.

Model-independent upper limits at 95% confidence level are presented on the production cross section, times branching ratio and acceptance. For resonant production, the limits are presented as a function of four-jet resonance mass between 2 and 9 TeV, for all accessible values of the ratio of the dijet to four-jet resonance masses. For non-resonant production, the limits are presented as a function of dijet resonance mass between 0.5 and 3 TeV.

Limits from the resonant search are compared to a model [22] of diquarks, which decay to pairs of vector-like quarks, which in-turn decay to a quark and a gluon. We present mass limits for all accessible values of the ratio of the vector-like quark to diquark masses, for a benchmark model where the diquark couplings to pairs of up quarks is 0.4, and the diquark couplings to pairs of vector-like quarks is 0.6. In particular, when we choose the ratio of the vector-like quark to diquark mass to be 0.25, motivated by the two observed events discussed above, we exclude at 95% CL diquarks with a mass less than 7.6 TeV (observed) and 7.8 TeV (expected).

Limits from the non-resonant search are compared to a model [23] of R-parity violating supersymmetry, with pair produced top squarks decaying to down and strange quarks. We exclude at 95% CL top squarks with masses between 0.50 and 0.52 TeV, and between 0.58 and 0.77 TeV (observed), and less than 0.67 TeV (expected), significantly extending the previous limit of 0.52 TeV [21]. In this case the most significant signal hypothesis occurs at an average dijet mass of 0.95 TeV, for which the local significance is 3.6 standard deviations and the global significance is 2.5 standard deviations.

References

[1] CMS Collaboration, "Search for high mass dijet resonances with a new background prediction method in proton-proton collisions at $\sqrt{s} = 13$ TeV", *JHEP* **05** (2020) 033, doi:10.1007/JHEP05(2020)033, arXiv:1911.03947.

[2] ATLAS Collaboration, "Search for new resonances in mass distributions of jet pairs using 139 fb^{-1} of pp collisions at $\sqrt{s} = 13$ TeV with the ATLAS detector", *JHEP* **03** (2020) 145, doi:10.1007/JHEP03(2020)145, arXiv:1910.08447.

[3] CMS Collaboration, "Search for narrow and broad dijet resonances in proton-proton collisions at $\sqrt{s} = 13$ TeV and constraints on dark matter mediators and other new particles", *JHEP* **08** (2018) 130, doi:10.1007/JHEP08(2018)130, arXiv:1806.00843.

[4] ATLAS Collaboration, "Search for new phenomena in dijet events using 37 fb^{-1} of pp collision data collected at $\sqrt{s}$ =13 TeV with the ATLAS detector", *Phys. Rev. D* **96** (2017) 052004, doi:10.1103/PhysRevD.96.052004, arXiv:1703.09127.

[5] CMS Collaboration, "Search for dijet resonances in proton-proton collisions at $\sqrt{s}$ = 13 TeV and constraints on dark matter and other models", *Phys. Lett. B* **769** (2017) 520, doi:10.1016/j.physletb.2017.02.012, arXiv:1611.03568.

[6] CMS Collaboration, "Search for narrow resonances decaying to dijets in proton-proton collisions at $\sqrt{s} = 13$ TeV", *Phys. Rev. Lett.* **116** (2016) 071801, doi:10.1103/PhysRevLett.116.071801, arXiv:1512.01224.

[7] ATLAS Collaboration, "Search for new phenomena in dijet mass and angular distributions from pp collisions at $\sqrt{s} = 13$ TeV with the ATLAS detector", *Phys. Lett. B* **754** (2016) 302, doi:10.1016/j.physletb.2016.01.032, arXiv:1512.01530.

[8] CMS Collaboration, "Search for narrow resonances in dijet final states at $\sqrt{s} = 8$ TeV with the novel CMS technique of data scouting", *Phys. Rev. Lett.* **117** (2016) 031802, doi:10.1103/PhysRevLett.117.031802, arXiv:1604.08907.

[9] CMS Collaboration, "Search for resonances and quantum black holes using dijet mass spectra in proton-proton collisions at $\sqrt{s} = 8$ TeV", *Phys. Rev. D* **91** (2015) 052009, doi:10.1103/PhysRevD.91.052009, arXiv:1501.04198.

[10] ATLAS Collaboration, "Search for new phenomena in the dijet mass distribution using pp collision data at $\sqrt{s} = 8$ TeV with the ATLAS detector", *Phys. Rev. D* **91** (2015) 052007, doi:10.1103/PhysRevD.91.052007, arXiv:1407.1376.

[11] CMS Collaboration, "Search for narrow resonances using the dijet mass spectrum in pp collisions at $\sqrt{s}$ = 8 TeV", *Phys. Rev. D* **87** (2013) 114015, doi:10.1103/PhysRevD.87.114015, arXiv:1302.4794.

[12] CMS Collaboration, "Search for narrow resonances and quantum black holes in inclusive and b-tagged dijet mass spectra from pp collisions at $\sqrt{s} = 7$ TeV", *JHEP* **01** (2013) 013, doi:10.1007/JHEP01(2013)013, arXiv:1210.2387.

[13] ATLAS Collaboration, "Search for new physics in the dijet mass distribution using 1 fb^{-1} of pp collision data at $\sqrt{s}$ = 7 TeV collected by the ATLAS detector", *Phys. Lett. B* **708** (2012) 37, doi:10.1016/j.physletb.2012.01.035, arXiv:1108.6311.

[14] ATLAS Collaboration, "ATLAS search for new phenomena in dijet mass and angular distributions using pp collisions at $\sqrt{s} = 7$ TeV", *JHEP* **01** (2013) 029, doi:10.1007/JHEP01(2013)029, arXiv:1210.1718.

[15] CMS Collaboration, "Search for resonances in the dijet mass spectrum from 7 TeV pp collisions at CMS", *Phys. Lett. B* **704** (2011) 123, doi:10.1016/j.physletb.2011.09.015, arXiv:1107.4771.

[16] ATLAS Collaboration, "Search for new physics in dijet mass and angular distributions in pp collisions at $\sqrt{s} = 7$ TeV measured with the ATLAS detector", *New J. Phys.* **13** (2011) 053044, doi:10.1088/1367-2630/13/5/053044, arXiv:1103.3864.

[17] CMS Collaboration, "Search for dijet resonances in 7 TeV pp collisions at CMS", *Phys. Rev. Lett.* **105** (2010) 211801, doi:10.1103/PhysRevLett.105.211801, arXiv:1010.0203. [Erratum doi:10.1103/PhysRevLett.106.029902].

[18] ATLAS Collaboration, "Search for new particles in two-jet final states in 7 TeV proton-proton collisions with the ATLAS detector at the LHC", *Phys. Rev. Lett.* **105** (2010) 161801, doi:10.1103/PhysRevLett.105.161801, arXiv:1008.2461.

[19] R. M. Harris and K. Kousouris, "Searches for Dijet Resonances at Hadron Colliders", *Int. J. Mod. Phys. A* **26** (2011) 5005–5055, doi:10.1142/S0217751X11054905, arXiv:1110.5302.

[20] ATLAS Collaboration, "Dijet resonance search with weak supervision using $\sqrt{s} = 13$ TeV pp collisions in the ATLAS detector", *Phys. Rev. Lett.* **125** (2020) 131801, doi:10.1103/PhysRevLett.125.131801, arXiv:2005.02983.

[21] CMS Collaboration, "Search for pair-produced resonances decaying to quark pairs in proton-proton collisions at $\sqrt{s} = 13$ TeV", *Phys. Rev. D* **98** (2018) 112014, doi:10.1103/PhysRevD.98.112014, arXiv:1808.03124.

[22] B. A. Dobrescu, R. M. Harris, and J. Isaacson, "Ultraheavy resonances at the LHC: beyond the QCD background", arXiv:1810.09429.

[23] R. Barbier et al., "R-parity violating supersymmetry", *Phys. Rept.* **420** (2005) 1, doi:10.1016/j.physrep.2005.08.006, arXiv:hep-ph/0406039.

[24] ATLAS Collaboration, "A search for pair-produced resonances in four-jet final states at $\sqrt{s} = 13$ TeV with the ATLAS detector", *Eur. Phys. J. C* **78** (2018) 250, doi:10.1140/epjc/s10052-018-5693-4, arXiv:1710.07171.

[25] CMS Collaboration, "Search for pair-produced resonances decaying to jet pairs in proton–proton collisions at $\sqrt{s} = 8$ TeV", *Phys. Lett. B* **747** (2015) 98, doi:10.1016/j.physletb.2015.04.045, arXiv:1412.7706.

[26] ATLAS Collaboration, "A search for top squarks with R-parity-violating decays to all-hadronic final states with the ATLAS detector in $\sqrt{s}$ = 8 TeV proton-proton collisions", *JHEP* **06** (2016) 067, doi:10.1007/JHEP06(2016)067, arXiv:1601.07453.

[27] CMS Collaboration, "Search for Pair-Produced Dijet Resonances in Four-Jet Final States in pp Collisions at $\sqrt{s}$=7 TeV", *Phys. Rev. Lett.* **110** (2013) 141802, doi:10.1103/PhysRevLett.110.141802, arXiv:1302.0531.

[28] ATLAS Collaboration, "Search for pair-produced massive coloured scalars in four-jet final states with the ATLAS detector in proton-proton collisions at $\sqrt{s} = 7$ TeV", *Eur. Phys. J. C* **73** (2013) 2263, doi:10.1140/epjc/s10052-012-2263-z, arXiv:1210.4826.

[29] CMS Collaboration, "The CMS experiment at the CERN LHC", *JINST* **3** (2008) S08004, doi:10.1088/1748-0221/3/08/S08004.

[30] CMS Collaboration, "Particle-flow reconstruction and global event description with the CMS detector", *JINST* **12** (2017) P10003, doi:10.1088/1748-0221/12/10/P10003, arXiv:1706.04965.

[31] M. Cacciari and G. P. Salam, "Dispelling the N^3 myth for the k_t jet-finder", *Phys. Lett. B* **641** (2006) 57, doi:10.1016/j.physletb.2006.08.037, arXiv:hep-ph/0512210.

[32] M. Cacciari, G. P. Salam, and G. Soyez, "The anti-k_T jet clustering algorithm", *JHEP* **04** (2008) 063, doi:10.1088/1126-6708/2008/04/063, arXiv:0802.1189.

[33] M. Cacciari, G. P. Salam, and G. Soyez, "FastJet user manual", *Eur. Phys. J. C* **72** (2012) 1896, doi:10.1140/epjc/s10052-012-1896-2, arXiv:1111.6097.

[34] M. Cacciari and G. P. Salam, "Pileup subtraction using jet areas", *Phys. Lett. B* **659** (2008) 119, doi:10.1016/j.physletb.2007.09.077, arXiv:0707.1378.

[35] CMS Collaboration, "Jet energy scale and resolution in the CMS experiment in pp collisions at 8 TeV", *JINST* **12** (2017) P02014, doi:10.1088/1748-0221/12/02/P02014, arXiv:1607.03663.

[36] CMS Collaboration, "The CMS trigger system", *JINST* **12** (2017) P01020, doi:10.1088/1748-0221/12/01/P01020, arXiv:1609.02366.

[37] CMS Collaboration, "Jet algorithms performance in 13 TeV data", CMS Physics Analysis Summary CMS-PAS-JME-16-003, CERN, Geneva, 2017.

[38] J. Alwall et al., "MadGraph 5 : Going Beyond", *JHEP* **1106** (2011) 128, doi:10.1007/JHEP06(2011)128, arXiv:1106.0522.

[39] J. A. Evans and Y. Kats, "LHC Coverage of RPV MSSM with Light Stops", *JHEP* **1304** (2013) 028, doi:10.1007/JHEP04(2013)028, arXiv:1209.0764.

[40] T. Sjöstrand et al., "An introduction to PYTHIA 8.2", *Comput. Phys. Commun.* **191** (2015) 159, doi:10.1016/j.cpc.2015.01.024, arXiv:1410.3012.

[41] GEANT 4 Collaboration, "Geant4 – a simulation toolkit", *Nucl. Instr. and Methods A* **506** (2003) 250, doi:10.1016/S0168-9002(03)01368-8.

[42] CMS Collaboration, "Event generator tunes obtained from underlying event and multiparton scattering measurements", *Eur. Phys. J. C* **76** (2016) 155, doi:10.1140/epjc/s10052-016-3988-x, arXiv:1512.00815.

[43] P. Skands, S. Carrazza, and J. Rojo, "Tuning PYTHIA 8.1: the Monash 2013 tune", *Eur. Phys. J. C* **74** (2014) 3024, doi:10.1140/epjc/s10052-014-3024-y, arXiv:1404.5630.

[44] NNPDF Collaboration, "Parton distributions with LHC data", *Nucl. Phys. B* **867** (2013) 244, doi:10.1016/j.nuclphysb.2012.10.003, arXiv:1207.1303.

[45] CDF Collaboration, "Search for new particles decaying into dijets in proton-antiproton collisions at $\sqrt{s} = 1.96$ TeV", *Phys. Rev. D* **79** (2009) 112002, doi:10.1103/PhysRevD.79.112002, arXiv:0812.4036.

[46] CMS Collaboration, "Precision luminosity measurement in proton-proton collisions at $\sqrt{s} = 13$ TeV in 2015 and 2016 at CMS", 2021. arXiv:2104.01927. Submitted to *Eur. Phys. J. C*.

[47] CMS Collaboration, "CMS luminosity measurements for the 2017 data taking period", CMS Physics Analysis Summary CMS-PAS-LUM-17-004, CERN, Geneva, 2017.

[48] CMS Collaboration, "CMS luminosity measurements for the 2018 data taking period", CMS Physics Analysis Summary CMS-PAS-LUM-18-002, CERN, Geneva, 2017.

[49] P. D. Dauncey, M. Kenzie, N. Wardle, and G. J. Davies, "Handling uncertainties in background shapes: the discrete profiling method", *JINST* **10** (2015) P04015, doi:10.1088/1748-0221/10/04/P04015, arXiv:1408.6865.

[50] T. Junk, "Confidence level computation for combining searches with small statistics", *Nucl. Instr. Meth. A* **434** (1999) 435, doi:10.1016/S0168-9002(99)00498-2, arXiv:hep-ex/9902006.

[51] A. L. Read, "Presentation of search results: the CL_s technique", *J. Phys. G* **28** (2002) 2693, doi:10.1088/0954-3899/28/10/313.

[52] LHC Higgs Combination Group, "Procedure for the LHC Higgs boson search combination in Summer 2011", Technical Report CMS-NOTE-2011-005, ATL-PHYS-PUB-2011-11, CERN, Geneva, 2011.

[53] G. Cowan, K. Cranmer, E. Gross, and O. Vitells, "Asymptotic formulae for likelihood-based tests of new physics", *Eur. Phys. J. C* **71** (2011) 1554, doi:10.1140/epjc/s10052-011-1554-0, arXiv:1007.1727. [Erratum: doi:10.1140/epjc/s10052-013-2501-z].

[54] R. D. Cousins and V. L. Highland, "Incorporating systematic uncertainties into an upper limit", *Nucl. Instrum. Meth. A* **320** (1992) 331, doi:10.1016/0168-9002(92)90794-5.

[55] C. Borschensky et al., "Squark and gluino production cross sections in pp collisions at $\sqrt{s}$ = 13, 14, 33 and 100 TeV", *Eur. Phys. J.* **C74** (2014) 3174, doi:10.1140/epjc/s10052-014-3174-y, arXiv:1407.5066.

[56] W. Beenakker et al., "NLO+NLL squark and gluino production cross-sections with threshold-improved parton distributions", *Eur. Phys. J.* **C76** (2016), no. 2, 53, doi:10.1140/epjc/s10052-016-3892-4, arXiv:1510.00375.